Inorganic Chemistry

Article

pubs.acs.org/IC

Lanthanum Lead Oxide Hydroxide Nitrates with a Nonlinear Optical Effect

Genxiang Wang,[†,‡] Min Luo,[†] Chensheng Lin,[†] Ning Ye,*[,†,‡] Yuqiao Zhou,[†] and Wendan Cheng[†]

[†]Fujian Institute of Research on the Structure of Matter, Key Laboratory of Optoelectronic Materials Chemistry and Physics, Chinese Academy of Sciences, Fuzhou, Fujian 350002, P. R. China

[‡]College of Chemistry & Chemical Engineering, Fuzhou University, Shangjie, Minhou, Fuzhou, Fujian 350108, P. R. China

Supporting Information

ABSTRACT: Two new lanthanum lead oxide hydroxide nitrates with acentric structure, $[LaPb_8O(OH)_{10}(H_2O)](NO_3)_7$ (**1**) and $[LaPb_8O(OH)_{10}(H_2O)](NO_3)_7{\cdot}2H_2O$ (**2**), have been prepared under subcritical hydrothermal conditions and crystallize in the space groups of *Cc* and $P2_12_12_1$, respectively. The crystal structure of compound **1** consists of the novel $[LaPb_8O(OH)_{10}(H_2O)]^{7+}$ clusters regularly arranged along the *ab* plane with nitrate ions as the counterions around the clusters by Pb−O bonds, developing into a three-dimensional net framework, while the structure of compound **2** is composed of $[LaPb_8O(OH)_{10}(H_2O)]^{7+}$ clusters and $[NO_3]^-$ groups as the bridging groups, forming a three-dimensional net framework with crystallized water molecules filling in the gaps. The experiments confirmed that compound **1** is the residue of compound **2** after efflorenscence. Besides, the $[LaPb_8O(OH)_{10}(H_2O)]^{7+}$ clusters present mirror symmetry in structures of the two compounds. The second-harmonic-generation (SHG) measurements for the two nitrates indicate that the SHG responses for compounds **1** and **2** are 1.3 and 1.1 times that of KH_2PO_4, respectively. Theoretical calculations confirmed that the SHG efficiency of compounds **1** and **2** mainly arises from the NO_3^- groups in the structure.

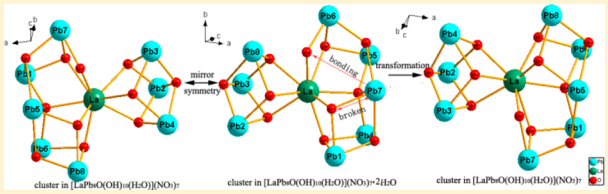

INTRODUCTION

The rapid development of laser science and technology has greatly promoted research of nonlinear-optical (NLO) materials.[1−18] Over the past decades, a lot of excellent NLO materials have been discovered, among which borates have been richly studied for the various structural possibilities of B atoms and the fact that the planar $[BO_3]^{3-}$ anionic group possesses the considerably large microscopic second-order susceptibility and moderate birefringence based on the Anionic Group Theory.[1,6,10−13,15−19] The unique advantages of the $[BO_3]^{3-}$ group motivate our interest in finding new NLO materials in carbonates and nitrates, in which $[CO_3]^{2-}$ and $[NO_3]^-$ anionic groups also have similar planar triangle structure with π-conjugated molecular orbitals. Because the carbonate system was studied, some relevant compounds with excellent NLO properties have constantly been discovered.[20−25] However, in contrast to the successful exploration of borate and carbonate, investigations of $[NO_3]^-$-containing materials with NLO properties have scarcely been systematically studied.[26−33]

For obtaining NLO materials with stronger second-harmonic-generation (SHG) effects, asymmetric building units,[34,35] such as distorted polyhedra with a d^0 cation center,[36−38] polar displacement of a d^{10} cation center,[39,40] and metal ions with ns^2 lone-pair electrons[41] are popularly introduced into molecular structures, which was successfully applied to design many good NLO materials.[36,42,43] The incorporation of the above acentric building units into nitrate systems may reinforce the SHG signal of materials. Other than the stereochemically active lone-pair effect of Pb^{2+}, lead-containing compounds are also special for their great structural variability,[44−49] which greatly prompts us to discover new NLO materials in lead nitrates. In our previous research, a series of nonaqueous lead oxide hydroxide nitrates with diverse structures have been synthesized by adjusting the pH values of the reaction systems.[33] Furthermore, on the basis of the fact that the types of lead nitrates may be enriched by introducing various cations and rare-earth-ion-containing crystal structures may present good SHG properties,[21,24,25] we try to introduce rare-earth ions into these compounds.

Therefore, a systematical study was carried out on the $Pb(NO_3)_2$−M_2O_3 (M = Sc, Y, Lu, La, Gd, Yb) system, giving rise to the discovery of two new NLO materials by hydrothermal reactions, $[LaPb_8O(OH)_{10}(H_2O)](NO_3)_7$ (**1**) and $[LaPb_8O(OH)_{10}(H_2O)](NO_3)_7{\cdot}2H_2O$ (**2**), respectively. Herein, we describe the syntheses, crystal structures, thermal behavior, spectra, NLO properties, and structure−property relationships of these two nitrates.

EXPERIMENTAL SECTION

Reagents. $Pb(NO_3)_2$ (99%) and La_2O_3 (99.99%) were procured from Sinopharm.

Received: September 10, 2014
Published: November 11, 2014

dx.doi.org/10.1021/ic502202a | *Inorg. Chem.* 2014, 53, 12584−12589

Syntheses. Crystals of $[LaPb_8O(OH)_{10}(H_2O)](NO_3)_7$ (**1**) and $[LaPb_8O(OH)_{10}(H_2O)](NO_3)_7{\cdot}2H_2O$ (**2**) were synthesized via the hydrothermal method using $Pb(NO_3)_2$ (0.828 g, 0.0025 mol) and H_2O (5 mL) with the addition of 0.407 g (0.00125 mol) and 0.814 g (0.0025 mol) of La_2O_3, respectively, charging in the Teflon autoclave (23 mL), heating at 180 °C for 4 days, and then slow cooling to ambient temperature at a rate of 3 °C/h. Colorless and transparent bulk crystals of compound **1** and white transparent rectangular bulk crystals of compound **2** were obtained in yields of about 72% and 80% (on the basis of Pb), respectively. The two products, nonaqueous at room temperature, were washed with ethanol and dried in air. It is worth noting that the crystals of **2** easily lose their crystal water molecules after exposure in air for several days, which leads to the white transparent rectangular bulk crystals changing into white nontransparent compounds. The phase and thermal behavior of the residue of compound **2** after efflorescence was also studied by powder X-ray diffraction (XRD) and thermal analysis.

Single-Crystal Structure Determination. Single-crystal XRD data for **1** and **2** were collected on a Rigaku Mercury CCD diffractometer with graphite-monochromatic Mo Kα radiation (λ = 0.71073 Å) at ambient temperature. The intensity data sets were corrected with the ω-scan technique. The data were integrated using the *CrystalClear* program, and the intensities were corrected for Lorentz polarization, air absorption, and absorption attributable to variation in the path length through the detector faceplate. Absorption corrections based on the multiscan technique were also applied. All structures were solved by direct methods and refined by full-matrix least-squares fitting on F^2 using *SHELX-97*.[50] All non-H atoms were refined with anisotropic constraints except atoms N1, N2, N3, N5, and N7 in compound **1** and O19, O28, N3, N5, O15, O35, O30, and N6 in compound **2**, which were refined with "ISOR" constraints. O1−O4, O6−O9, and O11−O12 in compound **1** and O2−O5, O7−O9, and O11−O13 in compound **2** are appointed as hydroxyl groups based on the requirements of charge-balance and bond-valence calculations, and their calculated bond valences are in the ranges of 1.17−1.5 and 1.24−1.40, respectively. Besides, O10 in compound **1** and O15, O27, O29, and O35 in compound **2** are designated as water molecules. The H atoms in the two compounds were not located, and all of the largest residual peaks in the final electron density map were close to the Pb atoms. The structures were checked for possible missing symmetry elements from the program *PLATON*,[51] but none were found. The crystallographic data for compounds **1** and **2** are summarized in Table 1. Atomic coordinates, isotropic displacement coefficients, and bond valence sums are listed in Tables S1 and S2 in the Supporting Information (SI) and bond distances in Tables S3 and S4 in the SI.

Powder XRD. XRD patterns for polycrystalline materials were carried out at room temperature on a PANalytical X'Pert PRO diffractometer equipped with Cu Kα radiation using continuous mode in the angular range of 2θ = 5−65° with a rate of 2θ = 1°/min. The experimented XRD patterns for these two compounds agree well with the calculated ones (Figure S1 in the SI).

Thermal Analysis. Thermogravimetric analysis (TGA) was conducted on a Netzsch STA 449C unit. The crystal samples (5−10 mg) were enclosed in Al_2O_3 crucibles and heated from room temperature to 800 °C at a rate of 10 °C/min under a constant flow of nitrogen gas.

UV−Vis Diffuse-Reflectance Spectroscopy. Optical diffuse-reflectance spectra were measured at room temperature with a PerkinElmer Lamda-900 UV−vis−near-IR spectrophotometer and scanned in the range of 190−2500 nm. The $BaSO_4$ plate was used as a standard (100% reflectance), and the reflectance values were converted to absorbance using the Kubelka−Munk function.[52,53] Absorption (K/S) data were calculated from the following Kubelka−Munk function: $F(R) = (1 - R)^2/2R = K/S$, where R is the reflectance, K is the absorption, and S is the scattering. In the K/S versus E plots, extrapolating the linear part of the rising curve to zero provides the onset of absorption.

IR Spectroscopy. The Fourier transform IR spectra were recorded on the Vertex 70 spectrometer by using KBr pellets in the range of 4000−400 cm^{-1}.

Table 1. Crystal Data and Structure Refinement for 1 and 2[a]

formula	$[LaPb_8O(OH)_{10}(H_2O)](NO_3)_7$	$[LaPb_8O(OH)_{10}(H_2O)](NO_3)_7{\cdot}2H_2O$
fw	2438.58	2470.48
cryst syst	monoclinic	orthorhombic
space group	*Cc*	$P2_12_12_1$
a (Å)	12.1152(11)	12.4804(11)
b (Å)	29.1414(18)	16.3805(15)
c (Å)	9.7545(8)	16.9652(18)
α (deg)	90	90
β (deg)	111.044(4)	90
γ (deg)	90	90
V ($Å^3$)	3214.2(4)	3468.3(6)
Z	4	4
ρ(calcd) (g/cm^3)	5.006	4.701
temperature (K)	293(2)	293(2)
λ (Å)	0.71073	0.71073
F(000)	4104	4168
θ (deg)	2.76−25.50	2.05−25.50
absolute structure param	0.00	0.011(14)
cryst size (mm^3)	0.5 × 0.4 × 0.1	0.2 × 0.15 × 0.1
completeness to θ = 25.50° (%)	99.5	99.8
R/R_w [$I > 2\sigma(I)$]	0.0658/0.1448	0.0519/0.1064
R/R_w (all data)	0.0710/0.1470	0.0617/0.1135
GOF on F^2	1.020	1.105

[a] $R(F) = \sum||F_o| - |F_c||/\sum|F_o|$. $R_w(F_o^2) = [\sum w(F_o^2 - F_c^2)^2/\sum w(F_o^2)^2]^1$.

SHG. Powder SHG signals were measured by means of the modified method of Kurtz and Perry.[54] Because SHG efficiencies are known to strongly depend on the particle size, polycrystalline samples were ground and sieved into six particle size ranges (25−45, 45−62, 62−75, 75−109, 109−150, and 150−212 μm). To make relevant comparisons with known SHG materials, crystalline KH_2PO_4 (KDP) was also ground and sieved into the same particle size ranges. The samples were pressed between glass microscope cover slides and secured with tape in 1-mm-thick aluminum holders each containing an 8-mm-diameter hole. Then the samples were placed in a light-tight box and irradiated with a pulsed laser one by one. The measurements were carried out on a Q-switched Nd:YAG laser at a wavelength of 1064 nm. A cutoff filter was used to limit background flash-lamp light on the sample. An interference filter (530 ± 10 nm) was used to select the second harmonic for detection with a photomultiplier tube attached to a RIGOL DS1052E 50-MHz oscilloscope. This procedure was then repeated using the standard NLO material KDP, and the ratio of the second-harmonic intensity outputs was calculated. No index-matching fluid was used in any of the experiments.

Computational Descriptions. Density functional theory (DFT) was applied to study the electronic structure and optical properties of **1** and **2** by using the *CASTEP* code.[55] The norm-conserving pseudopotentials were used to represent the ion cores. The valence electrons of the component elements were treated as H $1s^1$, O $2s^22p^4$, N $2s^22p^3$, La $5d^16s^2$, and Pb $5s^25p^65d^{10}6s^26p^2$. A generalized gradient approximation of the Perdew−Burke−Ernzerhof[56] scheme was used to describe the exchange-correlation XC function. Hydrogen atomic positions of the OH^- and H_2O groups were obtained by fixed-lattice constant optimization based on the X-ray crystal structure. All subsequent calculations were performed on this optimized geometry. The plane-wave energy cutoff was set as 700 eV. The self-consistent convergence of the total energy was set as 2.0×10^{-6} eV/atom. Up to 850 additional empty bands were used in the optical property calculations.

dx.doi.org/10.1021/ic502202a | *Inorg. Chem.* 2014, 53, 12584−12589

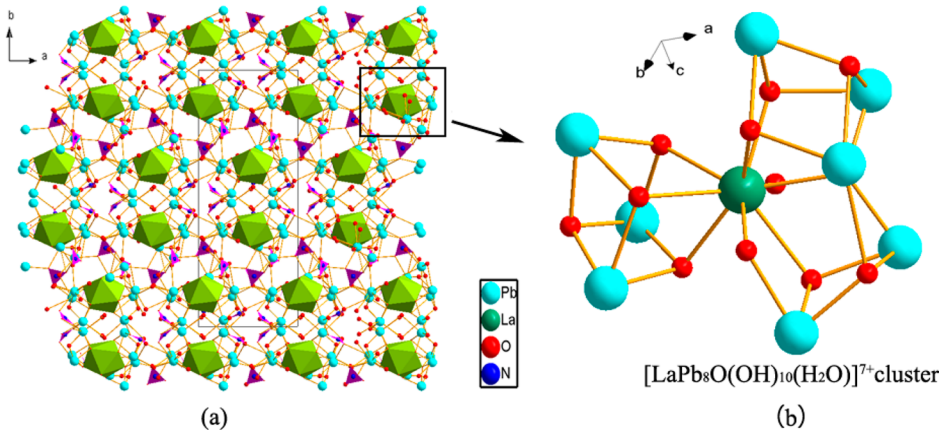

Figure 1. View of the structure of **1** down the *c* axis (a) and the $[LaPb_8O(OH)_{10}(H_2O)]^{7+}$ cluster in **1** (b).

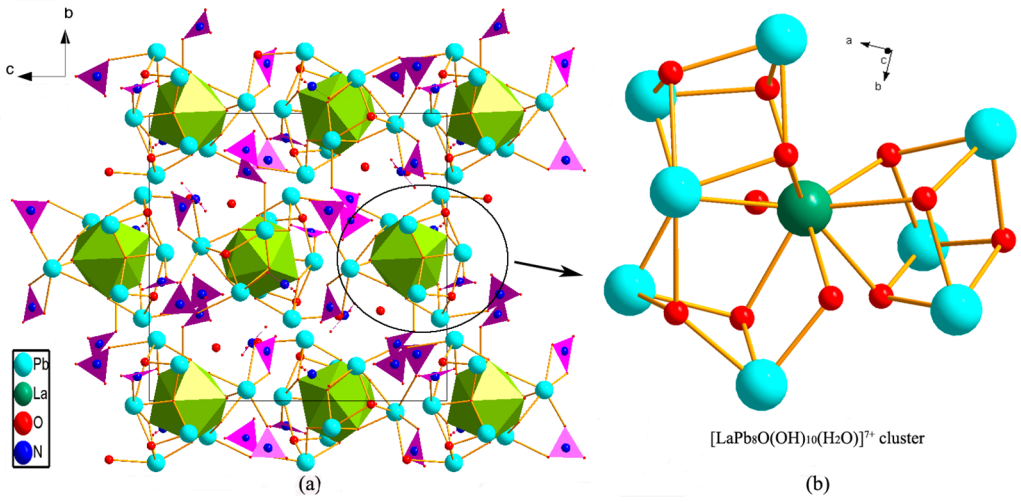

Figure 2. View of the structure of **2** down the *a* axis (a) and the $[LaPb_8O(OH)_{10}(H_2O)]^{7+}$ cluster in **2** (b).

RESULTS AND DISCUSSION

Thermal Properties. The TGA curve (Figure S2a in the SI) shows that the weight loss of **1** undergoes two steps in the range of 137−567 °C under a nitrogen atmosphere, resulting in a total weight loss of about 19.38% (calculated value 19.96%). The first step, with a weight loss about 4.03% in the range of 137−417 °C, can be assigned to the removal of six water molecules in the structure (calculated value 4.43%), arising from condensation of 10 hydroxyl groups and a coordinated water molecule. The second step presents a weight loss of about 15.35% (calculated value 15.53%) in the range of 417−567 °C, corresponding to decomposition of seven nitrate groups. The decomposition reaction is

$$[LaPb_8O(OH)_{10}(H_2O)](NO_3)_7 \longrightarrow LaPb_8O_6(NO_3)_7 + 6H_2O$$
$$\downarrow$$
$$8PbO + LaO_{3/2} + 7NO_2\uparrow + 7/4O_2\uparrow$$

The TGA studies for **2** (Figure S2b in the SI) show weight loss in three steps in the range of 25−568 °C owing to the weight losses of crystal water (25−74 °C), condensation of hydroxyl groups and a coordinated water molecule (75−429 °C), and release of NO_2 and O_2 (430−568 °C), corresponding to weight losses of 1.49% (calculated value 1.46%), 4.34% (calculated value 4.37%), and 14.62% (calculated value 15.30%), respectively. The decomposition reaction is

$$[LaPb_8O(OH)_{10}(H_2O)](NO_3)_7{\cdot}2H_2O$$
$$\downarrow$$
$$2H_2O + [LaPb_8O(OH)_{10}(H_2O)](NO_3)_7 \longrightarrow LaPb_8O_6(NO_3)_7 + 6H_2O$$
$$\downarrow$$
$$8PbO + LaO_{3/2} + 7NO_2\uparrow + 7/4O_2\uparrow$$

The residue of **2** after the dehydration procedure was **1**, as confirmed by powder XRD. Moreover, Figure S2c in the SI shows that the TGA curve for the residue after efflorescence of compound **2** is in well accordance with that of **1**.

Crystal Structure of 1. **1** crystallizes into a monoclinic crystal system with an acentric space group of *Cc*. The crystal structure of **1** consists of novel $[LaPb_8O(OH)_{10}(H_2O)]^{7+}$ clusters regularly arranged along the *ab* plane with nitrate ions as the counterions around the clusters by strong or weak Pb−O bonds, developing into a three-dimensional net framework (Figure 1a). The principal unit of the structure of compound **1** is the $[LaPb_8O(OH)_{10}(H_2O)]^{7+}$ cluster (Figure 1b), in which there are one unique La atom, coordinated with seven OH^- groups, one O atom as well as one water molecule, and eight Pb atoms bonded with the other three OH^- groups, forming three $[(OH)Pb_3]$ trigonal-pyramidal structures in which the OH^- group occupies the vertex. The cluster can be described as built from one nine-coordinated La polyhedron, $[LaO(OH)_7(H_2O)]$, capped by three $[(OH)Pb_3]$ trigonal-

dx.doi.org/10.1021/ic502202a | *Inorg. Chem.* 2014, 53, 12584−12589

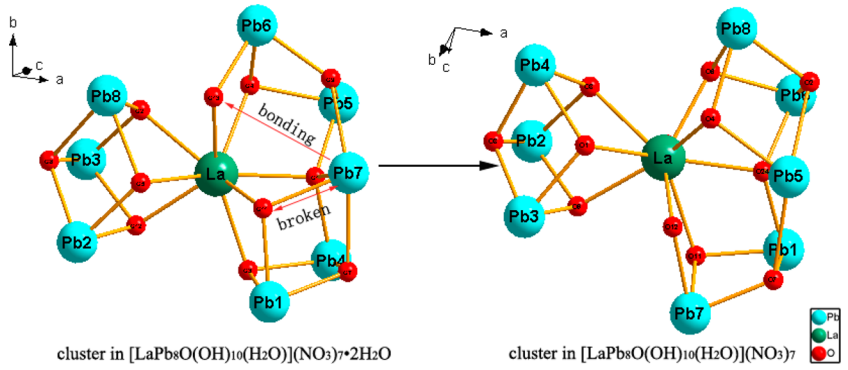

Figure 3. Variation of the cluster in **2** after its efflorescence.

pyramidal structures through Pb−O bonds and two of the trigonal-pyramidal structures sharing one Pb atom, forming two complete distorted cubane structures, $[LaPb_3(OH)_4]$, and an incomplete one in which one Pb−O bond is unconnected or seriously distorted by sharing a common La atom. The strong Pb−O bond lengths vary from 2.24(3) to 2.73(3) Å, the weak Pb−O bond lengths vary from 2.74(3) to 3.27(3) Å, and the bond lengths for La−O range from 2.42(3) to 2.71(3) Å. The calculated bond valence for Pb atoms is 1.86−2.24 and that for the La atom 3.14. In the structure, O10 was assigned to the coordinated water of the La atom with a calculated bond valence of 0.35, while O1−O4, O6−O9, and O11−O12 are assigned to hydroxyl groups, with the calculated bond valence ranging from 1.17 to 1.43. The $[NO_3]^-$ groups in the structure are disorderly aligned around the $[LaPb_8O(OH)_{10}(H_2O)]^{7+}$ clusters, which directly results in only a moderate contribution to the NLO effect of compound **1**. Some of these nitrate groups are slightly distorted. The N−O bond lengths in these planar $[NO_3]$ triangles are in the range of 1.11(4)−1.33(5) Å. The calculated bond valences for N atoms vary from 4.70 to 5.47.

Crystal Structure of 2. **2** crystallizes in the chiral and nonpolar space group $P2_12_12_1$ (No. 19) of the orthorhombic system. The structure of **2** is also composed of $[LaPb_8O(OH)_{10}(H_2O)]^{7+}$ clusters that existed in compound **1** and $[NO_3]^-$ groups as the bridging groups, forming a three-dimensional net framework with the crystallized water molecules filling in the gaps (Figure 2). It is worth noting that the $[LaPb_8O(OH)_{10}(H_2O)]^{7+}$ clusters in compound **2** show a mirror symmetry approximate to that in compound **1** (see Figures 1 and 2). The primary and secondary distances for the Pb−O bonds are in the ranges of 2.260(17)−2.753(18) and 2.781(2)−3.27(3) Å, respectively, and 2.527(17)−2.593(16) Å for the La−O bonds. The calculated bond valences for Pb atoms vary from 1.78 to 2.17, and it is 3.14 for La atom, which are in good agreement with the expected valence states. The unit cell figure shows that the $[NO_3]^-$ groups are in an unfavorable spacial alignment, leading to weak contribution to the SHG signals of the compound. The N−O bond lengths in these planar $[NO_3]$ triangles range from 1.16(4) to 1.30(3) Å. The calculated bond valences for N atoms are in the range of 4.83−5.48. In the structure, O15 is assigned to coordinated water of the La atom with a calculated bond valence of 0.33, and O35, O27, and O29 are assigned to crystallized water with a calculated bond valence of less than 0.5. While O2−O5, O7−O9, and O11−O13 are assigned as hydroxyl groups based on the requirements of charge-balance and bond-valence calculations, and their calculated bond valences are in the range of 1.24−1.40.

On the basis of the results in thermal analysis and XRD experiments, together with the above structural analysis, we propose structural evolution on the transformation of the dehydration process. Although the $[LaPb_8O(OH)_{10}(H_2O)]$ clusters in compounds **2** and **1** are related by mirror symmetry, they may convert to each other via slight displacements of Pb and O atoms. As shown in Figure 3, the breakage of the Pb7−O11 bond and the linkage of the Pb7−O13 bond in the cluster of compound **2** make the cluster change to those in compound **1**, which may be caused by escape of the adjacent crystalline water O27 close to Pb1 [the distance of Pb1−O27 is 2.74(2) Å]. Fundamentally, variation of the coordinated environment of Pb1 for the loss of crystaline water O27 causes recombination of the whole cluster. Escape of the other crystal water molecule in the structure of compound **2** induces the rearrangement of NO_3^- groups in this structure.

Optical Properties. Figure S3 in the SI displays the UV−vis diffuse reflectance spectra for **1** and **2**, which show little absorption in the ranges of 343−2500 and 346−2500 nm, and the cutoff edges are 343 and 346 nm, respectively. The results of optical diffuse-reflectance spectra suggest that both of the title compounds are wide-band-gap semiconductors[44] with optical band gaps of 3.612 and 3.576 eV, respectively.

IR spectra (Figure S4 in the SI) of the two title compounds were collected and show a few similar characteristic peaks. The absorption bands of **1** at around 3573 cm^{-1} and 1636 and 3416 cm^{-1} can be assigned to the H_2O and OH^- groups,[57] while the peaks of 1384 and 840 cm^{-1} can be assigned to the stretching vibration or bending vibrations of the NO_3^- groups; besides, 1028 cm^{-1} can be attributed to the symmetric and asymmetric stretches of the NO_3^- groups,[26,44] while the absorption peaks at 479 and 693 cm^{-1} can be assigned to the peaks of Pb−O. Some absorption peaks of the NO_3^- groups overlapped with the absorption peaks of Pb−O. Analogously, the peaks at 3560 cm^{-1}, 1650 and 3400 cm^{-1}, and 1384 and 840 cm^{-1} for **2** also confirm the existence of H_2O, OH^-, and NO_3^- groups, respectively, and the absorption peaks at 491 and 705 cm^{-1} can be assigned to the peaks of Pb−O.

NLO Properties. Figure 4 presents the curves of the SHG signal for **1** and **2**, which suggests that the materials are phase-matching.[58] Compared respectively with the reference KDP sample, the SHG signal is measured to be about 1.3 and 1.1 times that of KDP for compounds **1** and **2**. These values are proportional to the squares of the nonlinear d_{eff} coefficient. Because the reported d_{36} coefficient for KDP is 0.39 pm/V,[59] the derived d_{eff} coefficients for compounds **1** and **2** are 0.51 and 0.43 pm/V, respectively.

dx.doi.org/10.1021/ic502202a | Inorg. Chem. 2014, 53, 12584−12589

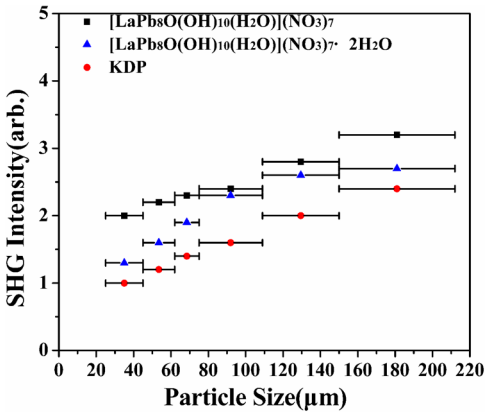

Figure 4. SHG measurements of **1** (black squares) and **2** ground crystals (blue triangles) with KDP (red circles) as the reference.

According to the anionic group theory,[60,61] it is the anionic groups in the acentric crystal structure that make dominant contributions to the main SHG coefficients ($[NO_3]$ in this case). Furthermore, on the basis of the theory[62] in the SI, the NLO coefficient $\chi^{(2)}_{ijk}$ is proportional to density of the $[NO_3]^-$ group (n/V) and the structural criterion (C; eqs 2 and 3 in the SI). Following the computing method used previously,[21,33] the calculated value of the C factor for **1** is about 32%, which comes from the contribution of g_{333} (Table S5 in the SI). The moderate C factor of compound **1** arises from the unfavorable arrangement of the $[NO_3]^-$ groups in the structure (Figure 1). For **2**, the calculated value of the C factor is around 31%, which comes from the contribution of g_{123} (Table S5 in the SI). The structural similarity of compounds **1** and **2** leads to a similar calculated value of the C factor, which is in accordance with the experimental results of the SHG measurements. To gain further insight into the SHG effects as determined by the arrangement and density of the NLO-active groups, the coefficients of the NLO effect for compounds **1** and **2** were calculated and compared with that of $[Pb_4(OH)_4](NO_3)_4$[33](Table 2).

Table 2. NLO Effects of $[Pb_4(OH)_4](NO_3)_4$,[33] 1, and 2

crystals (n)	SHG coefficient (visible) (×KDP)	structural criterion C	density of $[NO_3]$ (n/V) (Å^{-3})	(n/V)C (Å^{-3})
$[Pb_4(OH)_4](NO_3)_4$	0.7	0.17	0.0109	0.0018
1	1.3	0.32	0.0087	0.0028
2	1.1	0.31	0.0081	0.0025

Although the densities of $[NO_3]$ in compounds **1** and **2** are smaller than that in $[Pb_4(OH)_4](NO_3)_4$, the larger structural criterion C leads to the stronger SHG coefficient. Even so, the considerably low density (n/V = 0.00871 and 0.00807 Å^{-3} in compounds **1** and **2**, respectively) of $[NO_3]^-$, as well as moderate structural criterion values of the C factors, leads to the small NLO effect of the two new nitrates. As shown in Table 2, the above argument on the structure−property correlations is in good agreement with the SHG measurements.

Besides, in order to understand the contribution from the lone-pair electrons of the Pb^{2+} cation to the NLO properties of these two nitrates, the local dipole moments[63−65] of PbO_n polyhedra in the two title compounds were calculated. The distance of Pb−O in PbO_n polyhedra is less than 3.3 Å.[32,45] The direction and magnitude of PbO_n polyhedra in **1** and **2** are shown in Tables S6 and S7 in the SI, respectively. Table S6 in the SI shows that the dipole moments of PbO_n polyhedra in compound **1** along the y axis are canceled and their vector sum is well-enhanced in the ac plane (Figure S5 in the SI), producing a dipole moment of 92.88 D in the unit cell, and the mean polarization is small, only 18.33% of optimal.[33] Table S7 in the SI shows that the dipole moments of PbO_n polyhedra in compound **2** along the x, y, and z axes are almost canceled completely, and the total local dipole moment approaches 0 D (Figure S6 in the SI). Therefore, the lone-pair electrons of the Pb^{2+} cation make almost no contribution to the NLO effect of the two nitrates. Also, the SHG effects of the two compounds mainly arise from the NO_3^- groups.

Theoretical Calculations. The band structures are presented in Figure S7 in the SI). Compounds **1** and **2** exhibit direct band gaps of 2.853 and 2.888 eV, respectively (experimental values: 3.612 and 3.576 eV). The calculated values are smaller than the experimental values because of the common underestimation of the band gap by the DFT method. The total and partial densities of states (DOS and PDOS) for **1** and **2** are presented in Figure S8 in the SI. Only the upper region of the valence band and the bottom of the conduction band are shown because the linear-optical and NLO properties are mainly determined by the states close to the Fermi energy level. At the energy range between −5 eV and the Fermi level, the DOS is mainly composed of the p orbital of $[NO_3]^-$. The conduction bands from the Fermi level to 5 eV are mainly composed of the p orbital of the $[NO_3]^-$ groups. Thus, the electron transition is mainly contributed by inside excitation of the $[NO_3]^-$ group. Because of the above analysis, the NLO effect of the two nitrates mainly stems from the $[NO_3]^-$ groups, but the inappropriate spatial arrangement and low density of $[NO_3]^-$ led to the small NLO effect of the two nitrates.

CONCLUSIONS

Two new lanthanum lead oxide hydroxide nitrates with noncentrosymmetric structure, **1** and **2**, have been prepared by the hydrothermal method. The structures of the two nitrates feature the $[LaPb_8O(OH)_{10}(H_2O)]^{7+}$ clusters, which present mirror symmetry in the two compounds. Compound **2** transforms to compound **1** via a dehydration procedure, which is confirmed by the studies of powder XRD and thermal analysis. The SHG test shows that the compounds exhibit SHG responses of about 1.3 and 1.1 times those of KDP for compounds **1** and **2**, respectively, which mainly stems from the contributions of NO_3 groups in the structures, and the cause of the considerable weak SHG signals has also been analyzed based on the theory calculations.

ASSOCIATED CONTENT

Supporting Information

Crystallorgraphic data in CIF format, direction and magnitude of PbO_n polyhedra in **1** and **2**, calculated and experimental XRD patterns, UV absorption and optical diffuse-reflectance spectra, IR and TG traces, calculated band structures and total and partial densities of states for **1** and **2**, as well as NLO theory. This material is available free of charge via the Internet at http://pubs.acs.org.

AUTHOR INFORMATION

Corresponding Author

*E-mail: nye@fjirsm.ac.cn.

Notes

The authors declare no competing financial interest.

■ ACKNOWLEDGMENTS

This research was supported by the National Natural Science Foundation of China (Grants 91222204 and 90922035), Main Direction Program of Knowledge Innovation of Chinese Academy of Sciences (Grant KJCX2-EW-H03-03), and Special Project of National Major Scientific Equipment Development of China (Grant 2012YQ120060).

■ REFERENCES

(1) Chen, C. T.; Wu, B. C.; Jiang, A. D.; You, G. M. *Sci. Sin., Ser. B* **1985**, *28*, 235−243.
(2) Dmitriev, V. G.; Gurzadyan, G. G.; Nikogosyan, D. N. *Handbook of Nonlinear Optical Crystals*; Springer: Berlin, 1991.
(3) Chen, C. T.; Wang, Y. B.; Wu, B. C.; Wu, K. C.; Zeng, W. L.; Yu, L. H. *Nature* **1995**, *373*, 322−324.
(4) Hagerman, M. E.; Poeppelmeier, K. R. *Chem. Mater.* **1995**, *7*, 602−621.
(5) Becker, P. *Adv. Mater.* **1998**, *10*, 979−992.
(6) Wu, H. P.; Pan, S. L.; Poeppelmeier, K. R.; Li, H. Y.; Jia, D. Z.; Chen, Z. H.; Fan, X. Y.; Yang, Y.; Rondinelli, J. M.; Luo, H. S. *J. Am. Chem. Soc.* **2011**, *133*, 7786−7790.
(7) Boyd, G. D.; Buehler, E.; Storz, F. G. *Appl. Phys. Lett.* **1971**, *18*, 301−304.
(8) Liao, J. H.; Marking, G. M.; Hsu, K. F.; Matsushita, Y.; Ewbank, M. D.; Borwick, R.; Cunningham, P.; Rosker, M. J.; Kanatzidis, M. G. *J. Am. Chem. Soc.* **2003**, *125*, 9484−9493.
(9) Zhang, Q.; Chung, I.; Jang, J. I.; Ketterson, J. B.; Kanatzidis, M. G. *J. Am. Chem. Soc.* **2009**, *131*, 9896−9897.
(10) Wang, S. C.; Ye, N.; Li, W.; Zhao, D. *J. Am. Chem. Soc.* **2010**, *132*, 8779−8786.
(11) Yu, H. W.; Wu, H. P.; Pan, S. L.; Yang, Z. H.; Su, X.; Zhang, F. F. *J. Mater. Chem.* **2012**, *22*, 9665−9670.
(12) Huang, H. W.; Liu, L. J.; Jin, S. F.; Yao, W. J.; Zhang, Y. H.; Chen, C. T. *J. Am. Chem. Soc.* **2013**, *135*, 18319−18322.
(13) Wang, S. C.; Ye, N. *J. Am. Chem. Soc.* **2011**, *133*, 11458−11461.
(14) Xu, X.; Hu, C. L.; Kong, F.; Zhang, J. H.; Mao, J. G.; Sun, J. L. *Inorg. Chem.* **2013**, *52*, 5831−5837.
(15) Huang, H. W.; Yao, J. Y.; Lin, Z. S.; Wang, X. Y.; He, R.; Yao, W. J.; Zhai, N. X.; Chen, C. T. *Angew. Chem.* **2011**, *123*, 10456−10456.
(16) Zou, G. H.; Ma, Z. J.; Wu, K. C.; Ye, N. *J. Mater. Chem.* **2012**, *22*, 19911−19918.
(17) Yu, H. W.; Wu, H. P.; Pan, S. L.; Yang, Z. H.; Hou, X. L.; Su, X.; Jing, Q.; Poeppelmeier, K. R.; Rondinelli, J. M. *J. Am. Chem. Soc.* **2014**, *136*, 1264−1267.
(18) Chen, C. T.; Wu, Y. C.; Jiang, A. D.; Wu, B. C.; You, G. M.; Li, R. K.; Lin, S. J. *J. Opt. Soc. Am. B* **1989**, *6*, 616−621.
(19) Mei, L. F.; Wang, Y. B.; Chen, C. T.; Wu, B. C. *J. Appl. Phys.* **1993**, *74*, 7014−7015.
(20) Zou, G. H.; Ye, N.; Huang, L.; Lin, X. S. *J. Am. Chem. Soc.* **2011**, *133*, 20001−20007.
(21) Luo, M.; Ye, N.; Zou, G. H.; Lin, C. S.; Cheng, W. D. *Chem. Mater.* **2013**, *25*, 3147−3153.
(22) Tran, T. T.; Halasyamani, P. S. *Inorg. Chem.* **2013**, *52*, 2466−2473.
(23) Zou, G. H.; Huang, L.; Ye, N.; Lin, C. S.; Cheng, W. D.; Huang, H. *J. Am. Chem. Soc.* **2013**, *135*, 18560−18566.
(24) Luo, M.; Lin, C. S.; Zou, G. H.; Ye, N.; Cheng, W. D. *CrystEngComm* **2014**, *16*, 4414−4421.
(25) Luo, M.; Wang, G. X.; Lin, C. S.; Ye, N.; Zhou, Y. Q.; Cheng, W. D. *Inorg. Chem.* **2014**, *53*, 8098−8104.
(26) Wang, C. P.; Liu, Q.; Li, Z. H. *Cryst. Res. Technol.* **2011**, *46*, 655−658.
(27) Held, P.; Hellwig, H.; Ruhle, S.; Bohaty, L. *J. Appl. Crystallogr.* **2000**, *33*, 372−379.
(28) Bohatý, L.; Becker, P. *Cryst. Res. Technol.* **2009**, *44*, 1131−1138.
(29) Xue, D. F.; Zhang, S. Y. *Mol. Phys.* **1998**, *93*, 411−415.
(30) Ebbers, C. A.; DeLoach, L. D.; Webb, M.; Eimerl, D.; Velsko, S. P.; Keszler, D. A. *IEEE J. Quantum Electron.* **1993**, *29*, 497−507.
(31) Gasparri, G. F.; Nardelli, M.; Fermi, F. *Proc. Indian Acad. Sci. (Chem. Sci.)* **1984**, *93*, 283−293.
(32) Chang, L. X.; Wang, L.; Su, X.; Pan, S. L.; Hailili, R.; Yu, H. W.; Yang, Z. H. *Inorg. Chem.* **2014**, *53*, 3320−3325.
(33) Wang, G. X.; Luo, M.; Ye, N.; Lin, C. S.; Cheng, W. D. *Inorg. Chem.* **2014**, *53*, 5222−52228.
(34) Halasyamani, P. S.; Poeppelmeier, K. R. *Chem. Mater.* **1998**, *10*, 2753−2769.
(35) Ye, H. Y.; Fu, D. W.; Zhang, Y.; Zhang, W.; Xiong, R. G.; Huang, S. D. *J. Am. Chem. Soc.* **2008**, *131*, 42−43.
(36) Ra, H. S.; Ok, K. M.; Halasyamani, P. S. *J. Am. Chem. Soc.* **2003**, *125*, 7764−7765.
(37) Sykora, R. E.; Ok, K. M.; Halasyamani, P. S.; Albrecht-Schmitt, T. E. *J. Am. Chem. Soc.* **2002**, *124*, 1951−1957.
(38) Chi, E. O.; Ok, K. M.; Porter, Y.; Halasyamani, P. S. *Chem. Mater.* **2006**, *18*, 2070−2074.
(39) Zhang, W. L.; Cheng, W. D.; Zhang, H.; Geng, L.; Lin, C. S.; He, Z. Z. *J. Am. Chem. Soc.* **2010**, *132*, 1508−1509.
(40) Inaguma, Y.; Yoshida, M.; Katsumata, T. *J. Am. Chem. Soc.* **2008**, *130*, 6704−6705.
(41) Phanon, D.; Gautier-Luneau, I. *Angew. Chem., Int. Ed.* **2007**, *46*, 8488−8491.
(42) Huang, Y. Z.; Wu, L. M.; Wu, X. T.; Li, L. H.; Chen, L.; Zhang, Y. F. *J. Am. Chem. Soc.* **2010**, *132*, 12788−12789.
(43) Sun, C. F.; Hu, C. L.; Xu, X.; Ling, J. B.; Hu, T.; Kong, F.; Long, X. F.; Mao, J. G. *J. Am. Chem. Soc.* **2009**, *131*, 9486−9487.
(44) Song, J. L.; Hu, C. L.; Xu, X.; Kong, F.; Mao, J. G. *Inorg. Chem.* **2013**, *52*, 8979−8986.
(45) Grimes, S. M.; Johnston, S. R.; Abrahams, I. *J. Chem. Soc., Dalton Trans.* **1995**, *12*, 2081−2086.
(46) Li, Y. P.; Krivovichev, S. V.; Burns, P. C. *J. Solid State Chem.* **2000**, *153*, 365−370.
(47) Li, Y. P.; Krivovichev, S. V.; Burns, P. C. *J. Solid State Chem.* **2001**, *158*, 74−77.
(48) Krivovichev, S. V.; Li, Y. P.; Burns, P. C. *J. Solid State Chem.* **2001**, *158*, 78−81.
(49) Kolitsch, U.; Tillmanns, E. *Mineral. Mag.* **2003**, *67*, 79−93.
(50) Sheldrick, G. M. *Acta Crystallogr., Sect. A: Found. Crystallogr.* **2008**, *64*, 112−122.
(51) Spek, A. *J. Appl. Crystallogr.* **2003**, *36*, 7−13.
(52) Wendlandt, W. M.; Hecht, H. G. *Reflectance Spectroscopy*; Interscience: New York, 1966.
(53) Tauc, J. *Mater. Res. Bull.* **1970**, *5*, 721−729.
(54) Kurtz, S. K.; Perry, T. T. *J. Appl. Phys.* **1968**, *39*, 3798−3813.
(55) Segall, M. D. L.; Philip, J. D.; Probert, M. J.; Pickard, C. J.; Hasnip, P. J.; Clark, S. J.; Payne, M. C. *J. Phys.: Condens. Matter* **2002**, *14*, 2717−2744.
(56) Perdew, J. P.; Burke, K.; Ernzerhof, M. *Phys. Rev. Lett.* **1996**, *77*, 3865−3868.
(57) Xu, X.; Yang, B. P.; Huang, C.; Mao, J. G. *Inorg. Chem.* **2014**, *53*, 1756−1763.
(58) Kurtz, S. K.; Perry, T. T. *J. Appl. Phys.* **1968**, *39*, 3798−3813.
(59) Eckardt, R. C.; Masuda, H.; Fan, Y. X.; Byer, R. L. *IEEE J. Quantum Electron.* **1990**, *26*, 922−933.
(60) Chen, C. T. *Sci. Sin. (Engl. Ed.)* **1979**, *22*, 756−776.
(61) Chen, C. T.; Liu, G. Z. *Annu. Rev. Mater. Res.* **1986**, *16*, 203−243.
(62) Ye, N.; Chen, Q. X.; Wu, B. C.; Chen, C. T. *J. Appl. Phys.* **1998**, *84*, 555−558.
(63) Godby, R. W.; Schluter, M.; Sham, L. J. *Phys. Rev. B: Condens. Matter Mater. Phys.* **1987**, *36*, 6497−6500.
(64) Terki, R.; Bertrand, G.; Aourag, H. *Microelectron. Eng.* **2005**, *81*, 514−523.
(65) Sun, C. F.; Hu, C. L.; Mao, J. G. *Chem. Commun.* **2012**, *48*, 4220−4222.